Fractals in the 3-Body Problem Via Symplectic Integration

Daniel Hemberger
Department of Astronomy, Cornell University
109 Space Sciences Building, Ithaca, New York 14853

James A. Walsh
Department of Mathematics, Oberlin College
10 N. Professor St., Oberlin, OH 44074

1. Introduction. The statement of the n-body problem is tantalizingly simple: Given the present positions and velocities of n celestial bodies, predict their motions under Newton's inverse square law of gravitation for all future time and deduce them for all past time.

This simplicity belies the fact that efforts to solve this problem, beginning particularly with the work of Henri Poincaré in the late 19th century, essentially led to the creation of the field of dynamical systems. The study of the n-body problem remains an active area of research (see, for example, [17]).

It is intriguing to consider how Poincaré's research might have benefited had he access to modern computing capabilities. That he was able to discern what are now known as fractals and chaotic behavior in the 3-body problem [19] using only paper, pencil, and mental acumen (ferocious though it was) is remarkable.

It is safe to assume, nonetheless, that even Poincaré would have gained further insight into fractal geometry and chaotic dynamics had he access to modern numerical integration algorithms. In particular, given that the equations of motion for the 3-body problem are *Hamiltonian* in nature, it is now clear that he would have used a *symplectic integration algorithm* to numerically compute solutions.

The development of new numerical integration algorithms for Hamiltonian systems of ODEs and, more generally, for systems of equations admitting a geometric structure, began in the 1990s and continues to this day [6]. These algorithms have proven far superior to Runge-Kutta type algorithms in approximating the long-term, global, qualitative behavior of solutions. It is fun to imagine Poincaré staring at

a phase space on a computer screen, as might a modern dynamicist, searching for insights which could lead to another new theorem.

In this paper we investigate fractals arising in the 3-body problem. We do this via the simplified, low-dimensional variation of this problem known as the trilinear 3-body problem [15]. Along the way we define what Hamiltonian systems of ODEs and symplectic maps are. We also present an example of a symplectic integration algorithm (SIA) and illustrate why an SIA is ideally suited for generating the fractal structure which can arise in phase space for Hamiltonian systems of equations.

Many approaches to designing SIAs involve the use of generating functions or Lie algebraic techniques ([5], [10]). Our presentation of this type of algorithm is more elementary and well-suited for undergraduates. This article is in fact an extension of a research project undertaken by the first author in his junior year while a member of an introductory dynamical systems course taught by the second author. Hemberger's SIA code was written and executed in *Matlab*.

We conclude this paper with a comparison of the performance of this SIA vis-à-vis Runge-Kutta methods. The superiority of the symplectic algorithm is striking (see Figures 9, 10, and 11, for example).

2. Hamiltonian Systems. Hamiltonian systems of equations often arise when modeling physical systems in which there is a conserved quantity such as energy. Their importance in the study of ODEs is indicated by their inclusion in standard sophomore-level ODE texts such as [3] and [4]. Indeed, all students of introductory ODEs have seen at least one Hamiltonian system, namely that derived from the undamped, unforced harmonic oscillator:

$$m\ddot{q} + kq = 0, \qquad m, k > 0. \tag{1}$$

In equation (1), $q = q(t)$ is the position of a block of mass m, attached to a spring with spring constant k, relative to equilibrium at time t, while dots represent differentiation with respect to t (one dot for the first derivative, two dots for the second derivative).

Hamiltonian systems are first-order systems of ODEs. So the trick is to introduce a second variable $p = m\dot{q}$ (the *conjugate momentum*), so that $\dot{p} = m\ddot{q} = -kq$, which converts (1) into the first-order system

$$\begin{aligned} \dot{q} &= \tfrac{1}{m}p \\ \dot{p} &= -kq. \end{aligned} \tag{2}$$

Solutions to (2) are curves in the (q, p)-phase plane (Figure 1(b)); one can then recover the time evolution of the position of the block by projecting onto the q-coordinate while moving along a solution curve.

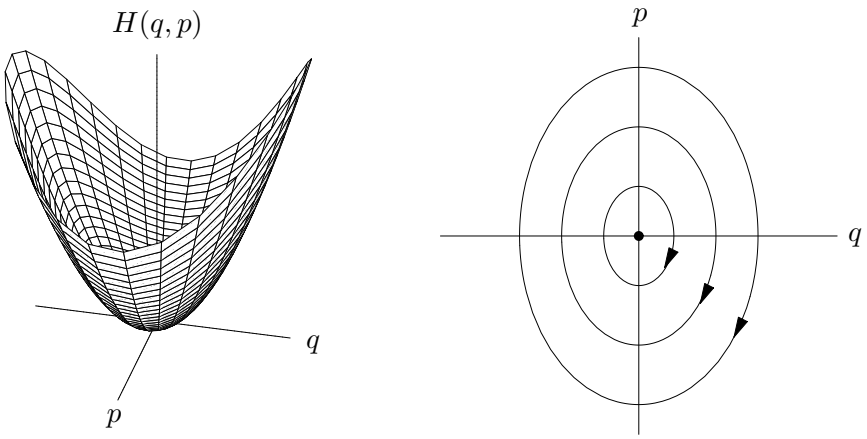

Figure 1. (a) The Hamiltonian $H(q,p) = \frac{1}{2m}p^2 + \frac{k}{2}q^2$. (b) The (q,p)-phase plane for the harmonic oscillator ($m = 1, k = 2$). Level sets of the Hamiltonian provide solution curves in the (q,p)-phase plane.

How are the curves in this phase plane generated? Note that the scalar function $H : \mathbb{R} \times \mathbb{R} \to \mathbb{R},\ H(q,p) = \frac{1}{2m}p^2 + \frac{k}{2}q^2$ satisfies

$$\begin{aligned} \dot{q} &= \tfrac{\partial H}{\partial p} \\ \dot{p} &= -\tfrac{\partial H}{\partial q}. \end{aligned} \tag{3}$$

By the multivariable chain rule this in turn implies that, given a solution $(q(t), p(t))$ to system (2),

$$\frac{d}{dt}H(q(t),p(t)) = \frac{\partial H}{\partial q}\frac{dq}{dt} + \frac{\partial H}{\partial p}\frac{dp}{dt} = -\dot{p}\,\dot{q} + \dot{q}\,\dot{p} = 0.$$

Hence the function H is constant along solution curves of system (2) or, put another way, solutions to (2) lie on level sets of H (Figure 1). This is an exceedingly nice happenstance as one can then sketch solution curves in the (q,p)-phase plane without recourse to finding actual formulas for $q(t)$ and $p(t)$.

A function H satisfying system (3) is called a *Hamiltonian function*. In this example, interpreting $A(p) = \frac{1}{2m}p^2$ and $U(q) = \frac{k}{2}q^2$ as the kinetic and potential energies, respectively, we see that total energy is conserved along solution curves to system (2). Were we to add damping or external forcing to the model, this Hamiltonian structure would be lost as energy would no longer be conserved.

Our second example of a well-known Hamiltonian system is provided by the undamped, unforced ideal pendulum. In this model, $q = q(t)$ is the angle the rod forms

with the vertical, g is the gravitational constant, and L is the length of the (massless) rod. The model ODE [3] is

$$mL\ddot{q} + mg\sin q = 0. \tag{4}$$

Again letting $p = m\dot{q}$, we convert (4) into the first-order system

$$\begin{cases} \dot{q} = \frac{1}{m}p \\ \dot{p} = -\frac{mg}{L}\sin q, \end{cases} \tag{5}$$

for which solution curves are sketched in Figure 2(b).

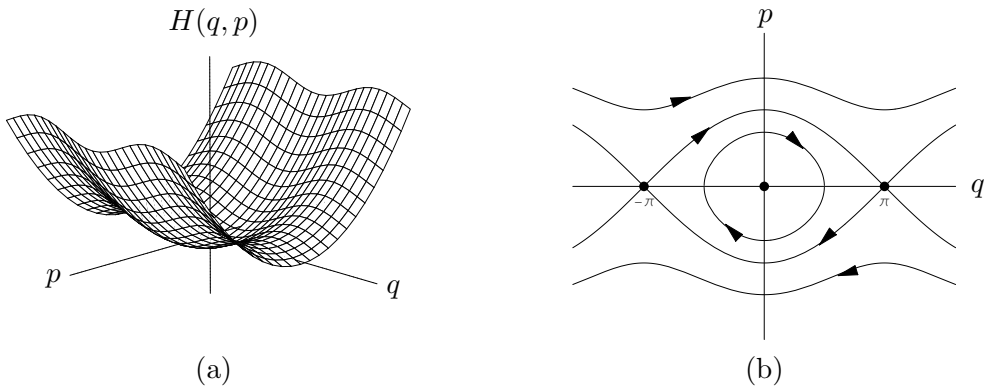

Figure 2. (a) The Hamiltonian $H(q,p) = \frac{1}{2m}p^2 - \frac{mg}{L}\cos q$. (b) The (q,p)-phase plane for the ideal pendulum ($m = 1, L = g$). Level sets of the Hamiltonian provide solution curves in the (q,p)-phase plane.

With neither damping nor forcing present, one might expect energy to be conserved for this model. This is indeed the case: the Hamiltonian function $H : \mathbb{R}\times\mathbb{R} \to \mathbb{R}$, $H(q,p) = A(p)+U(q) = \frac{1}{2m}p^2 - \frac{mg}{L}\cos q$ satisfies equation (3). Hence level curves of H provide solution curves to (5).

More generally, let $(\mathbf{q},\mathbf{p}) = (q_1,\ldots,q_d,p_1,\ldots,p_d)$ be a point in $\mathbb{R}^d \times \mathbb{R}^d$. If $H : \mathbb{R}^d \times \mathbb{R}^d \to \mathbb{R}$ is a C^2 function, then the Hamiltonian system of ODEs with Hamiltonian H is given by the system of $2d$ first-order equations

$$\dot{q}_i = \frac{\partial H}{\partial p_i}, \qquad \dot{p}_i = -\frac{\partial H}{\partial q_i}, \quad i = 1,\ldots,d. \tag{6}$$

The integer d is the *number of degrees of freedom*, while $\mathbb{R}^d \times \mathbb{R}^d$ is the *phase space*. In applications to mechanics, the $\mathbf{q}$ variables are often generalized coordinates, the $\mathbf{p}$ variables are conjugate generalized momenta, and H represents the total mechanical

energy. The mass on a spring and ideal pendulum models each have one degree of freedom with phase space $\mathbb{R} \times \mathbb{R}$.

One implication of the Poincaré-Bendixson Theorem [14] is that chaotic behavior cannot occur in systems of first-order ODEs with phase space $\mathbb{R} \times \mathbb{R}$. As for the n-body problem, fractals and chaos do not occur when $n = 2$: J. Bernoulli proved in 1710 that the path followed by one body with respect to the other always lies along a conic section. At least 3 bodies are thus needed to potentially have fractal geometry and chaotic dynamics present in the n-body problem.

We now introduce a relatively simple variant of the 3-body problem and describe the inherent fractal structure Poincaré would have seen had he a modern workstation running a symplectic integration algorithm.

3. The Trilinear 3-Body Problem. The trilinear 3-body problem is arguably the simplest entrée into the study of the 3-body problem. The model yields a low-dimensional system which has the added benefit that no two bodies ever collide, ensuring that the corresponding vector field has no singularities.

Place bodies on each of three parallel lines in the plane as in Figure 3. The top and bottom lines are each separated from the center line by $\epsilon/2$, for some fixed $\epsilon > 0$. Let m_i and x_i denote the mass and (horizontal) position, measured from a chosen origin, of the ith body, $i = 1, 2, 3$. Let the bodies move without friction under Newton's inverse square law of gravitation. Given an initial state, what happens?

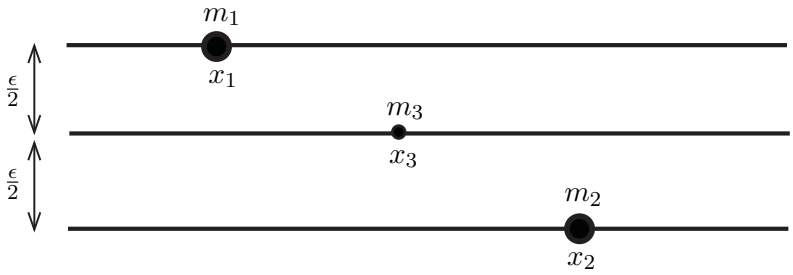

Figure 3. The trilinear 3-body model.

We begin by deriving the model differential equations. Though the equations may appear a bit unwieldy and yield an $\mathbb{R}^3 \times \mathbb{R}^3$ phase space, we will see that our study of model behavior can be reduced to two dimensions and iteration of a planar map.

Referring to Figure 4, we see that the distance from body 1 to body 2 is

$$D = \sqrt{(x_2 - x_1)^2 + \epsilon^2}.$$

By Newton's inverse square law of gravitation, the component of the gravitational force exerted by m_2 on m_1 in the direction of motion of m_1 is

$$\|\mathbf{F}\| \cos\theta = \frac{m_1 m_2}{D^2} \cdot \frac{x_2 - x_1}{D} = \frac{m_1 m_2 (x_2 - x_1)}{((x_2 - x_1)^2 + \epsilon^2)^{3/2}}.$$

We have set the gravitational constant G to equal 1 in the above, which can be accomplished by changing the unit of mass [16].

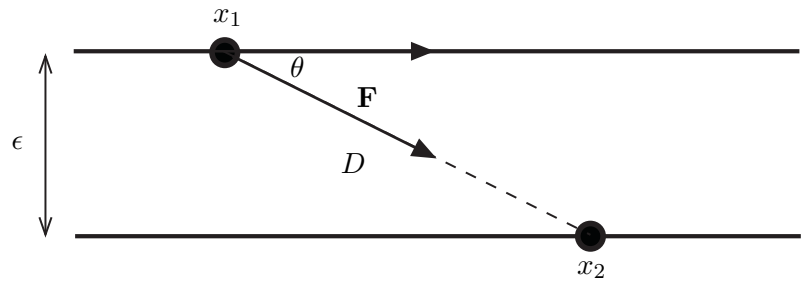

$$D = \sqrt{(x_2 - x_1)^2 + \epsilon^2}$$

Figure 4. Deriving the model equations.

In a similar fashion, the component of the force m_3 exerts on m_1 in the direction of motion of m_1 is

$$\frac{m_1 m_3}{(\sqrt{(x_3 - x_1)^2 + (\epsilon/2)^2})^2} \cdot \frac{x_3 - x_1}{\sqrt{(x_3 - x_1)^2 + (\epsilon/2)^2}} = \frac{m_1 m_3 (x_3 - x_1)}{((x_3 - x_1)^2 + \epsilon^2/4)^{3/2}}.$$

Computing the four remaining components of the forces one body exerts on another and using Newton's second law yields the system of second-order equations

$$\begin{aligned}
m_1 \ddot{x}_1 &= \frac{m_1 m_2 (x_2 - x_1)}{((x_2 - x_1)^2 + \epsilon^2)^{3/2}} + \frac{m_1 m_3 (x_3 - x_1)}{((x_3 - x_1)^2 + \epsilon^2/4)^{3/2}} \\
m_2 \ddot{x}_2 &= \frac{m_1 m_2 (x_1 - x_2)}{((x_1 - x_2)^2 + \epsilon^2)^{3/2}} + \frac{m_2 m_3 (x_3 - x_2)}{((x_3 - x_2)^2 + \epsilon^2/4)^{3/2}} \qquad (7) \\
m_3 \ddot{x}_3 &= \frac{m_1 m_3 (x_1 - x_3)}{((x_1 - x_3)^2 + \epsilon^2/4)^{3/2}} + \frac{m_2 m_3 (x_2 - x_3)}{((x_2 - x_3)^2 + \epsilon^2/4)^{3/2}}.
\end{aligned}$$

Introducing the variables $q_i = x_i$ and $p_i = m_i \dot{q}_i$, $i = 1, 2, 3$, converts (7) into the first-order system

$$\dot{q}_i = \tfrac{1}{m_i} p_i, \;\; i = 1, 2, 3, \quad \text{and}$$

$$\begin{aligned}
\dot{p}_1 &= \frac{m_1 m_2 (q_2 - q_1)}{((q_2 - q_1)^2 + \epsilon^2)^{3/2}} + \frac{m_1 m_3 (q_3 - q_1)}{((q_3 - q_1)^2 + \epsilon^2/4)^{3/2}} \\
\dot{p}_2 &= \frac{m_1 m_2 (q_1 - q_2)}{((q_1 - q_2)^2 + \epsilon^2)^{3/2}} + \frac{m_2 m_3 (q_3 - q_2)}{((q_3 - q_2)^2 + \epsilon^2/4)^{3/2}} \\
\dot{p}_3 &= \frac{m_1 m_3 (q_1 - q_3)}{((q_1 - q_3)^2 + \epsilon^2/4)^{3/2}} + \frac{m_2 m_3 (q_2 - q_3)}{((q_2 - q_3)^2 + \epsilon^2/4)^{3/2}}.
\end{aligned} \tag{8}$$

Note that system (8) is defined for all $(\mathbf{q}, \mathbf{p})$ in $\mathbb{R}^3 \times \mathbb{R}^3$. Moreover, one can easily check that $H : \mathbb{R}^3 \times \mathbb{R}^3 \to \mathbb{R}$,

$$H(\mathbf{q}, \mathbf{p}) = A(\mathbf{p}) + U(\mathbf{q}) =$$

$$\sum_{i=1}^{3} \frac{1}{2m_i} p_i^2 - \frac{m_1 m_2}{\sqrt{(q_2 - q_1)^2 + \epsilon^2}} - \frac{m_1 m_3}{\sqrt{(q_3 - q_1)^2 + \epsilon^2/4}} - \frac{m_2 m_3}{\sqrt{(q_2 - q_3)^2 + \epsilon^2/4}}$$

is a Hamiltonian function for system (8).

Solutions to (8) lie in 6-dimensional phase space $\mathbb{R}^3 \times \mathbb{R}^3$. We note, however, that Poincaré simplified his study of the 3-body problem by assuming that one body was small enough so that the gravitational force it exerts can be neglected, and that the two larger masses (called *primaries*) move in circles in a plane $\mathcal{P}$ about their center of mass. This simplified problem is known as the restricted, planar, circular 3-body problem, the goal of which is to understand the behavior of the small body as it moves in $\mathcal{P}$ under the gravitational influence of the primaries.

We follow Poincaré's lead in simplifying the trilinear 3-body problem. As shown in [15], one can assume the center of mass is fixed at the origin (accomplished via a change of coordinates). This implies

$$\frac{m_1 q_1 + m_2 q_2 + m_3 q_3}{m_1 + m_2 + m_3} = 0, \quad \text{that is,} \;\; m_1 q_1 + m_2 q_2 + m_3 q_3 = 0. \tag{9}$$

We also consider a restricted problem: body 3 is so small that the primaries do not feel its gravitational effect. Setting $m_3 = 0$ in (9) yields $m_1 q_1 + m_2 q_2 = 0$. If we assume further that $m_1 = m_2 = m$, then $q_1 = -q_2$ and $p_1 = -p_2$ for all time, so that the positions and velocities of the primaries are always symmetric about the origin. Once we know $q_1(t)$ and $p_1(t)$, we then have $q_2(t)$ and $p_2(t)$. Hence we can reduce (8) to the 4-dimensional system (we set $m = 1$ in all that follows)

$$\dot{q}_1 = p_1, \;\; \dot{q}_3 = p_3, \quad \text{and}$$

$$\dot{p}_1 = -\frac{2q_1}{(4q_1^2+\epsilon^2)^{3/2}} \tag{10}$$

$$\dot{p}_3 = \frac{q_1-q_3}{((q_1-q_3)^2+\epsilon^2/4)^{3/2}} - \frac{q_1+q_3}{((q_1+q_3)^2+\epsilon^2/4)^{3/2}}.$$

Note further that the $\dot{q}_1$- and $\dot{p}_1$-equations in system (10) decouple. In addition,

$$H_1(q_1,p_1) = \frac{1}{2}p_1^2 - \frac{1}{2\sqrt{4q_1^2+\epsilon^2}}$$

is a Hamiltonian function for this subsystem, leading to the (q_1,p_1)-phase plane sketched in Figure 5.

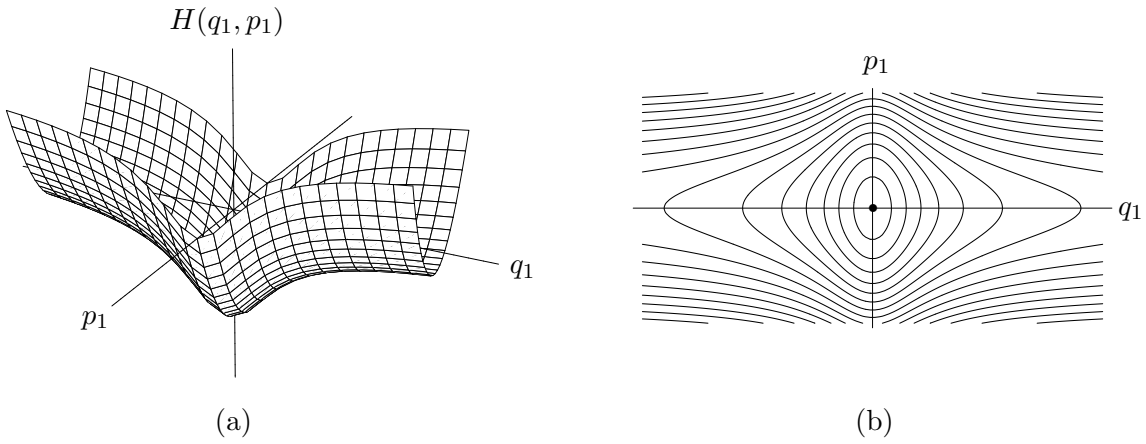

Figure 5. (a) The Hamiltonian $H(q_1,p_1) = \frac{1}{2}p_1^2 - 1/(2\sqrt{4q_1^2+\epsilon^2})$. (b) The (q_1,p_1)-phase plane (the periodic orbits are moving clockwise). Level sets of the Hamiltonian provide solution curves in the (q_1,p_1)-phase plane.

We see that if $p_1(0)$ is small enough, then the motion of m_1 (and so also of m_2) is periodic. We have arrived at the analog of Poincaré's reduction in his study of the 3-body problem: determine the behavior of the small center body as the primaries move periodically about their center of mass.

The periodicity of the primaries lends itself nicely to consideration of a *first return* (or *Poincaré*) map. We will sample the position and velocity of the small body each time the velocity of body 1 equals zero. This yields a mapping P_a, defined on the (q_3,p_3)-plane, and reduces our 6-dimensional system (8) to the study of the orbits of a

planar map. (The parameter a represents the amplitude of the large mass oscillation, as discussed in section 7.)

Our study will be aided greatly by the use of a symplectic integration algorithm. This type of algorithm is appropriate as the Poincaré map P_a introduced above for the trilinear 3-body problem makes use of a symplectic map in its very definition.

4. What is a Symplectic Map? The approach to symplectic maps taken here, which is ideally suited for undergraduates, follows that found in [21, Ch. 2] and [11, Ch. 6].

Let $\mathbf{v} = (v_1, v_2)^T$ and $\mathbf{w} = (w_1, w_2)^T$ be vectors in the plane. Recall from linear algebra that the area of the parallelogram spanned by $\mathbf{v}$ and $\mathbf{w}$ is $\|\mathbf{v} \times \mathbf{w}\| = |v_1 w_2 - w_1 v_2|$. Symplectic maps are concerned with *oriented* area: the oriented area of the parallelogram spanned by $\mathbf{v}$ and $\mathbf{w}$ is $v_1 w_2 - w_1 v_2$, while the oriented area of the parallelogram spanned by $\mathbf{w}$ and $\mathbf{v}$ is $w_1 v_2 - v_1 w_2$.

For reasons which will soon become clear, we observe that the oriented area of the parallelogram spanned by $\mathbf{v}$ and $\mathbf{w}$ is given by $\mathbf{v}^T J \mathbf{w}$, where $J = \left[\begin{smallmatrix} 0 & 1 \\ -1 & 0 \end{smallmatrix}\right]$:

$$\mathbf{v}^T J \mathbf{w} = \begin{bmatrix} v_1 & v_2 \end{bmatrix} \begin{bmatrix} 0 & 1 \\ -1 & 0 \end{bmatrix} \begin{bmatrix} w_1 \\ w_2 \end{bmatrix} = \begin{bmatrix} v_1 & v_2 \end{bmatrix} \begin{bmatrix} w_2 \\ -w_1 \end{bmatrix} = v_1 w_2 - w_1 v_2.$$

Let $\mathbf{L} : \mathbb{R} \times \mathbb{R} \to \mathbb{R} \times \mathbb{R}$ be a linear map, given by a 2×2 matrix L, and let P denote the parallelogram spanned by two vectors $\mathbf{v}$ and $\mathbf{w}$. Recall that $\mathbf{L}$ maps P to a parallelogram P' spanned by $L\mathbf{v}$ and $L\mathbf{w}$. Then $\mathbf{L}$ preserves oriented area if and only if $(L\mathbf{v})^T J (L\mathbf{w}) = \mathbf{v}^T J \mathbf{w}$ for all $\mathbf{v}$ and $\mathbf{w}$, that is, $L^T J L = J$.

Now let $\mathbf{f} : \mathbb{R} \times \mathbb{R} \to \mathbb{R} \times \mathbb{R}$, $\mathbf{f}(q, p) = (f_1(q, p), f_2(q, p))$, be a differentiable map. Let (q, p) be a point in $\mathbb{R} \times \mathbb{R}$, and let $\mathbf{v}$ and $\mathbf{w}$ be vectors sharing initial point (q, p). The map $\mathbf{f}$ takes the parallelogram spanned by $\mathbf{v}$ and $\mathbf{w}$ to a curved parallelogram $\mathbf{f}(P)$ as in Figure 6. We may approximate $\mathbf{f}(P)$ by the parallelogram P' spanned by the vectors $\mathbf{f}'\mathbf{v}$ and $\mathbf{f}'\mathbf{w}$, where

$$\mathbf{f}' = \mathbf{f}'(q, p) = \frac{\partial(f_1, f_2)}{\partial(q, p)} = \begin{bmatrix} \frac{\partial f_1}{\partial q} & \frac{\partial f_1}{\partial p} \\ \frac{\partial f_2}{\partial q} & \frac{\partial f_2}{\partial p} \end{bmatrix}$$

is the Jacobian matrix. This leads to the following definition.

Definition. A differentiable map $\mathbf{f} : \mathbb{R} \times \mathbb{R} \to \mathbb{R} \times \mathbb{R}$ is *symplectic* if

$$\mathbf{f}'(q, p)^T J \, \mathbf{f}'(q, p) = J \quad \text{for all} \quad (q, p) \in \mathbb{R} \times \mathbb{R}.$$

By partitioning a given domain in $\mathbb{R} \times \mathbb{R}$ with ever-smaller parallelograms, we see that symplectic is equivalent to oriented area preserving when $d = 1$. Though it may

seem natural to generalize to "volume preserving" for the case $d > 1$, as we'll see symplectic means more than this.

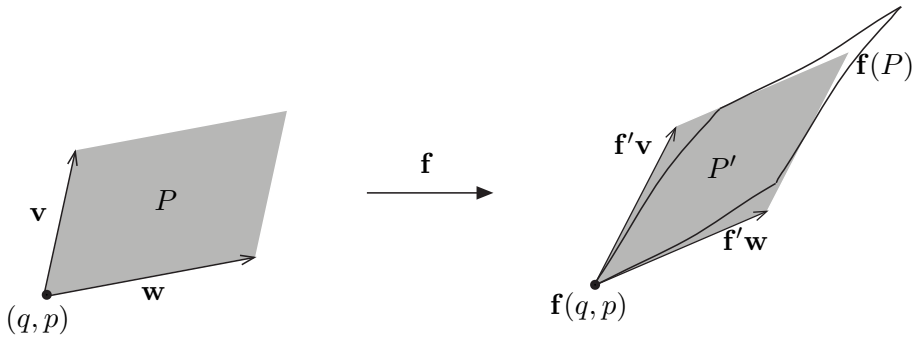

Figure 6

We introduce the definition for higher dimensions by first considering a linear map $\mathbf{L} : \mathbb{R}^d \times \mathbb{R}^d \to \mathbb{R}^d \times \mathbb{R}^d$ given by a $2d \times 2d$ matrix L. Let I denote the d-dimensional identity matrix, and set $J = \left[\begin{smallmatrix} 0 & I \\ -I & 0 \end{smallmatrix}\right]$. Given vectors $\mathbf{v}$ and $\mathbf{w}$ in $\mathbb{R}^d \times \mathbb{R}^d$, consider the parallelogram $P = \{\, t\mathbf{v} + s\mathbf{w} \,:\, t, s \in [0,1] \,\}$. The quantity $\mathbf{v}^T L \mathbf{w}$ represents the sum of the two-dimensional oriented areas of the d parallelograms resulting from the projections of P onto the (q_i, p_i)-coordinate planes, $i = 1, ..., d$.

Let's verify this when $d = 2$. Let $\mathbf{v} = (q_1^v, q_2^v, p_1^v, p_2^v)^T$ and let $\mathbf{w} = (q_1^w, q_2^w, p_1^w, p_2^w)^T$. We have

$$\mathbf{v}^T J \mathbf{w} = \begin{bmatrix} q_1^v & q_2^v & p_1^v & p_2^v \end{bmatrix} \begin{bmatrix} 0 & 0 & 1 & 0 \\ 0 & 0 & 0 & 1 \\ -1 & 0 & 0 & 0 \\ 0 & -1 & 0 & 0 \end{bmatrix} \begin{bmatrix} q_1^w \\ q_2^w \\ p_1^w \\ p_2^w \end{bmatrix} = \begin{bmatrix} q_1^v & q_2^v & p_1^v & p_2^v \end{bmatrix} \begin{bmatrix} p_1^w \\ p_2^w \\ -q_1^w \\ -q_2^w \end{bmatrix}$$

$$= q_1^v p_1^w + q_2^v p_2^w - q_1^w p_1^v - q_2^w p_2^v = \begin{vmatrix} q_1^v & p_1^v \\ q_1^w & p_1^w \end{vmatrix} + \begin{vmatrix} q_2^v & p_2^v \\ q_2^w & p_2^w \end{vmatrix}, \quad \text{as desired.}$$

A differentiable map $\mathbf{f} : \mathbb{R}^d \times \mathbb{R}^d \to \mathbb{R}^d \times \mathbb{R}^d$ is then defined to be *symplectic* if $\mathbf{f}'(\mathbf{q}, \mathbf{p})^T J \, \mathbf{f}'(\mathbf{q}, \mathbf{p}) = J$ for all $(\mathbf{q}, \mathbf{p}) \in \mathbb{R}^d \times \mathbb{R}^d$.

The notion of symplectic for $d > 1$ can be interpreted as follows. Consider an oriented surface Λ in $\mathbb{R}^d \times \mathbb{R}^d$. Let Λ_i denote the projections of Λ onto the (q_i, p_i)-coordinate planes, $i = 1, ..., d$. Let Λ_i' denote the projections of $\mathbf{f}(\Lambda)$ onto the (q_i, p_i)-coordinate planes. Using tangent parallelogram approximations, a symplectic map then has the property that the sum of the oriented areas of the Λ_i equals the sum of the oriented areas of the Λ_i'.

We consider an example furnished by the simple harmonic oscillator (2). Students of differential equations know the solution to (2) satisfying $(q(0), p(0)) = (q_0, p_0)$ is

$$\begin{bmatrix} q(t) \\ p(t) \end{bmatrix} = \begin{bmatrix} \cos \omega t & \frac{1}{m\omega} \sin \omega t \\ -m\omega \sin \omega t & \cos \omega t \end{bmatrix} \begin{bmatrix} q_0 \\ p_0 \end{bmatrix} = L_t \begin{bmatrix} q_0 \\ p_0 \end{bmatrix}, \tag{11}$$

where $\omega = \sqrt{k/m}$.

For *fixed* t, the above matrix defines a mapping $\mathbf{L}_t : \mathbb{R} \times \mathbb{R} \to \mathbb{R} \times \mathbb{R}$ which sends the point (q_0, p_0) to the value at time t of the solution to equation (2) with initial condition (q_0, p_0).

We claim the map $\mathbf{L}_t$ is symplectic. Since the map is linear (recall t is fixed), the Jacobian matrix at any (q_0, p_0) equals L_t. We compute

$$\begin{aligned} L_t^T J L_t &= \begin{bmatrix} \cos \omega t & -m\omega \sin \omega t \\ \frac{1}{m\omega} \sin \omega t & \cos \omega t \end{bmatrix} \begin{bmatrix} 0 & 1 \\ -1 & 0 \end{bmatrix} \begin{bmatrix} \cos \omega t & \frac{1}{m\omega} \sin \omega t \\ -m\omega \sin \omega t & \cos \omega t \end{bmatrix} \\ &= \begin{bmatrix} \cos \omega t & -m\omega \sin \omega t \\ \frac{1}{m\omega} \sin \omega t & \cos \omega t \end{bmatrix} \begin{bmatrix} -m\omega \sin \omega t & \cos \omega t \\ -\cos \omega t & -\frac{1}{m\omega} \sin \omega t \end{bmatrix} = \begin{bmatrix} 0 & 1 \\ -1 & 0 \end{bmatrix}. \end{aligned}$$

The reader may have noticed that for any t, $\det(L_t) = 1$. This implies the linear map $\mathbf{L}_t$ preserves oriented area which, as mentioned above, is the equivalent of symplectic in $\mathbb{R} \times \mathbb{R}$. For $d > 1$ volume preserving and symplectic are not equivalent. For example, consider the linear map $\mathbf{L}$ defined on $\mathbb{R}^2 \times \mathbb{R}^2$, given by the matrix

$$L = \begin{bmatrix} 1 & 1 & 0 & 0 \\ 0 & 1 & 0 & 0 \\ 0 & 0 & 1 & 0 \\ 0 & 0 & 0 & 1 \end{bmatrix}.$$

The map $\mathbf{L}$ preserves volume in $\mathbb{R}^4$ since $\det L = 1$. It is not symplectic, however, as a simple calculation shows

$$L^T J L = \begin{bmatrix} 0 & 0 & 1 & 0 \\ 0 & 0 & 1 & 1 \\ -1 & -1 & 0 & 0 \\ 0 & -1 & 0 & 0 \end{bmatrix} \neq J.$$

The harmonic oscillator example was also chosen to illustrate the fact that "time-t" maps arising from Hamiltonian systems of ODEs are *always* symplectic. We turn now to symplectic maps as the defining characteristic of Hamiltonian systems.

5. Hamiltonian flows and symplectic maps. Consider the first-order system of ODEs

$$\dot{\mathbf{x}} = \mathbf{f}(\mathbf{x}), \tag{12}$$

where $\mathbf{x} : \mathbb{R} \to \mathbb{R}^n$, $\mathbf{x}(t) = (x_1(t), ..., x_n(t))$, and $\mathbf{f} : \mathbb{R}^n \to \mathbb{R}^n$ is a C^1 vector field. The *flow* associated with system (12) is a function which maps $\mathbf{x}_0$ and a time t to the

value at time t of the solution to (12) having initial condition $\mathbf{x}_0 = \mathbf{x}(0)$. (We note t must be in the domain of the solution.)

More formally, the flow $\boldsymbol{\phi}(\mathbf{x}, t)$ is a mapping from $\mathbb{R}^n \times \mathbb{R}$ into $\mathbb{R}^n$ satisfying

(i) $\boldsymbol{\phi}(\mathbf{x}, 0) = \mathbf{x}$ for all $\mathbf{x} \in \mathbb{R}^n$;

(ii) $\boldsymbol{\phi}(\boldsymbol{\phi}(\mathbf{x}, t), s) = \boldsymbol{\phi}(\mathbf{x}, t + s)$ for all $\mathbf{x} \in \mathbb{R}^n$ and all $t, s \in \mathbb{R}$ for which both sides are defined; and

(iii) $\frac{\partial}{\partial t}\boldsymbol{\phi}(\mathbf{x}, t) = \mathbf{f}(\boldsymbol{\phi}(\mathbf{x}, t))$.

The flow is also denoted $\boldsymbol{\phi}_t(\mathbf{x})$. Property (iii) implies that if we hold $\mathbf{x}_0$ fixed, the function $t \mapsto \boldsymbol{\phi}(\mathbf{x}_0, t)$ is a solution of (12). Property (i) implies this solution also satisfies the initial condition $\mathbf{x}(0) = \mathbf{x}_0$. Finally, (ii) states that the flow gives rise to a group action (the group $(\mathbb{R}, +)$ is acting on $\mathbb{R}^n$).

We have previously seen an example of a flow, namely that corresponding to the harmonic oscillator and given in equation (11). Recall that for each t, $\boldsymbol{\phi}((q, p), t) = L_t(q, p)^T$ preserves area. It is indeed always the case that flows arising from Hamiltonian systems of ODEs preserve area in $\mathbb{R} \times \mathbb{R}$ and, more generally, preserve volume in $\mathbb{R}^d \times \mathbb{R}^d$ phase space. Intuitively, the transport of points in phase space by a Hamiltonian flow is akin to that of particles of an incompressible fluid flow.

More formally, volume preservation means that given any bounded domain $U \subset \mathbb{R}^d \times \mathbb{R}^d$ and any t for which $\boldsymbol{\phi}((\mathbf{q}, \mathbf{p}), t)$ exists for all $(\mathbf{q}, \mathbf{p})$ in U, $\mathrm{vol}(\boldsymbol{\phi}(U, t)) = \mathrm{vol}(U)$ (see Figure 7). This fact is a consequence of Liouville's Theorem ([11, p. 228], [12, p. 96]), since the vector field given by system (6)

$$\mathbf{f}(\mathbf{q}, \mathbf{p}) = \left(\frac{\partial H}{\partial p_1}, \frac{\partial H}{\partial p_2}, \ldots, \frac{\partial H}{\partial p_d}, -\frac{\partial H}{\partial q_1}, -\frac{\partial H}{\partial q_2}, \ldots, -\frac{\partial H}{\partial q_d}\right)^T$$

has divergence 0 due to the equality of second-order mixed partial derivatives:

$$\mathrm{div}\ \mathbf{f} = \sum_{i=1}^{d} \frac{\partial^2 H}{\partial q_i \partial p_i} + \sum_{i=1}^{d} \frac{-\partial^2 H}{\partial p_i \partial q_i} = 0.$$

There exist first-order systems of ODEs which are not Hamiltonian, yet for which the associated flow preserves volume. Thus, volume preservation is not a defining characteristic of Hamiltonian systems. Symplecticity, it turns out, is.

Theorem 1. [20] *Suppose $H : \mathbb{R}^d \times \mathbb{R}^d \to \mathbb{R}$ is a C^2 Hamiltonian function. Then for each fixed t, the corresponding flow $\boldsymbol{\phi}_t$ is a symplectic map wherever it is defined.*

We refer the reader to [11, §6.2] for a proof of Theorem 1.

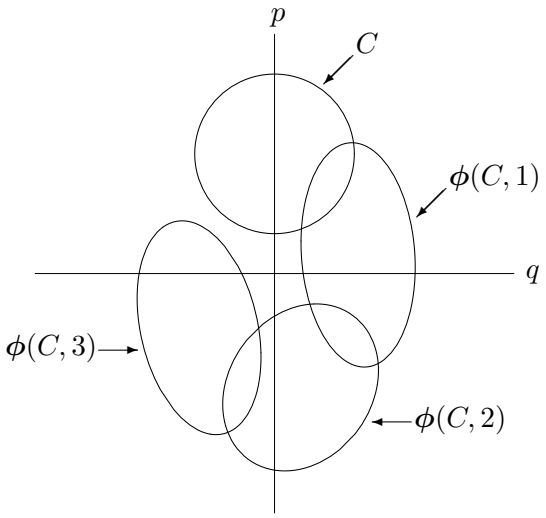

Figure 7. The harmonic oscillator flow: the areas enclosed by C and $\boldsymbol{\phi}(C,i),\ i=1,2,3$, are equal.

We see that in addition to preserving volume, a Hamiltonian flow must also define a symplectic map for fixed t. It is the converse of Theorem 1 which serves to distinguish between these two fundamental properties.

Theorem 2. Suppose $\mathbf{f} : \mathbb{R}^d \times \mathbb{R}^d \to \mathbb{R}^d \times \mathbb{R}^d$ *is a* C^2 *vector field. If the flow corresponding to the system* $\dot{\mathbf{x}} = \mathbf{f}(\mathbf{x})$ *is symplectic wherever it is defined, then this system is Hamiltonian.*

We see that symplecticity is both a stronger property than volume preservation and one which completely characterizes Hamiltonian flows.

Though we do not know of an elementary proof of Theorem 2, perhaps the $d = 1$ case will provide insight into its veracity. Suppose for fixed t the flow $\boldsymbol{\phi}_t$ associated with the system

$$\begin{aligned} \dot{q} &= f_1(q,p) \\ \dot{p} &= f_2(q,p) \end{aligned} \tag{13}$$

is symplectic. Recall that symplectic and oriented area preserving are equivalent in $\mathbb{R} \times \mathbb{R}$. Once again by Liouville's Theorem, the vector field $\mathbf{f} = (f_1, f_2)$ must have divergence 0. Hence $\frac{\partial f_1}{\partial q} + \frac{\partial f_2}{\partial p} = 0$, or $\frac{\partial f_1}{\partial q} = -\frac{\partial f_2}{\partial p}$, which is precisely the condition that guarantees system (13) is Hamiltonian in nature [3, §5.3]. A more sophisticated approach is clearly needed for $d > 1$; see [1, §40] or [11, §6.2].

In light of theorems 1 and 2, it is no surprise that symplectic maps have great potential when used to numerically integrate Hamiltonian systems of ODEs. In particular, they are ideally suited to generate global, qualitative structure in phase space

for the trilinear 3-body problem (Figures 9, 10, 11, and those following). We present one such *symplectic integration algorithm*, along with simulations, in the following sections.

6. A Symplectic Integration Algorithm. Standard integration algorithms are very useful when the goal is to obtain short-time, quantitative information. For systems exhibiting chaotic behavior, or fractal structure in phase space, long-time integrations are necessary. For these latter types of dynamical systems, standard integration algorithms are often unreliable.

We do not provide a comprehensive overview of symplectic integration algorithms (SIAs) in this article. There are many different SIAs, and the choice of which to use for a given integration is highly problem dependent. We focus here on one SIA, describe its development, and explain why it works so well. Readers interested in a more thorough treatment of this topic might consult the books [21] or [11], or the article [5].

Consider once again the harmonic oscillator (2), setting $k = m = 1$. Recall the total energy is given by $H(q,p) = \frac{1}{2}(p^2 + q^2)$. Euler's method with step size τ, given for this system by the mapping

$$\begin{bmatrix} q_{n+1} \\ p_{n+1} \end{bmatrix} = \begin{bmatrix} q_n + \tau p_n \\ p_n - \tau q_n \end{bmatrix} = \begin{bmatrix} 1 & \tau \\ -\tau & 1 \end{bmatrix} \begin{bmatrix} q_n \\ p_n \end{bmatrix} = L_\tau (q_n, p_n)^T, \tag{14}$$

is an integration algorithm which is *not* symplectic. To see this, simply compute

$$L_\tau^T J L_\tau = \begin{bmatrix} 0 & 1+\tau^2 \\ -(1+\tau^2) & 0 \end{bmatrix} \neq J.$$

Alternatively, observe that this algorithm *adds energy* to the system by a factor of $1 + \tau^2$ each iteration (see Figure 8):

$$H(q_{n+1}, p_{n+1}) = \frac{1}{2}\left((p_n - \tau q_n)^2 + (q_n + \tau p_n)^2\right) = (1+\tau^2) H(q_n, p_n).$$

It is this artificial increase (or, for other algorithms, damping) of energy which often makes long-time standard integrations of Hamiltonian systems spurious.

A slight adjustment to mapping (14), however, does yield the symplectic map

$$\begin{bmatrix} q_{n+1} \\ p_{n+1} \end{bmatrix} = \begin{bmatrix} 1-\tau^2 & \tau \\ -\tau & 1 \end{bmatrix} \begin{bmatrix} q_n \\ p_n \end{bmatrix} = M_\tau (q_n, p_n)^T. \tag{15}$$

A simple computation shows that $M_\tau^T J M_\tau = J$.

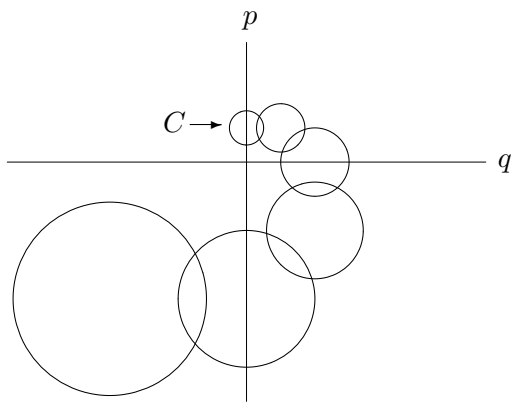

Figure 8. Euler's Method is not a symplectic algorithm. Pictured are successive images, moving clockwise, of a small circle C under iteration of Euler's Method for the harmonic oscillator with step size 1.

Mapping (15), of course, no longer preserves the Hamiltonian $H(q,p) = \frac{1}{2}(p^2+q^2)$. For the Hamiltonian

$$H(q,p) = \frac{1}{2}(p^2+q^2) - \frac{\tau}{2}pq, \tag{16}$$

however, it *is* the case that $H(q_{n+1},p_{n+1}) = H(q_n,p_n)$, as the reader is invited to check. Hence, map (15) *exactly solves* the Hamiltonian system given by (16). Starting with initial condition $(1,0)$, for example, map (15) will generate points on the ellipse $\frac{1}{2}(p^2+q^2) - \frac{\tau}{2}pq = \frac{1}{2}$, which differs from the exact solution $\frac{1}{2}(p^2+q^2) = \frac{1}{2}$ to system (2) only by a term of order 1 in τ. The energy error is bounded for all time (indeed, it is periodic) when using (15) to solve system (2). This is in contrast to Runge-Kutta type algorithms, for which energy error grows linearly with integration time [8]. For SIAs, energy error is always bounded and periodic, although phase error for periodic orbits can grow linearly with the number of periods [22].

This then is the advantage of an SIA: one uses a symplectic map to exactly solve a Hamiltonian which is close to the original Hamiltonian. While these algorithms have been particularly useful in carrying out long-time integrations of planetary orbits ([18], [23]), they are also used in many other settings ([7], [9], for example).

We now describe the SIA used to generate the images for the trilinear 3-body model in this article. This particular algorithm concerns *separable* Hamiltonians, of which those defining systems (2), (5) and (8) are examples. Separable Hamiltonians are generally of the form $H(\mathbf{q},\mathbf{p}) = A(\mathbf{p}) + U(\mathbf{q})$, and typically arise in physical systems in which there is no friction.

As this algorithm involves the composition of symplectic maps, we begin by noting that if $\mathbf{f}$ and $\mathbf{g}$ are symplectic maps, then so is $\mathbf{f}\circ\mathbf{g}$:

$$((\mathbf{f}\circ\mathbf{g})')^T\, J\, (\mathbf{f}\circ\mathbf{g})' = (\mathbf{f}'\mathbf{g}')^T\, J\, (\mathbf{f}'\mathbf{g}') = (\mathbf{g}')^T(\mathbf{f}')^T\, J\, \mathbf{f}'\mathbf{g}' = (\mathbf{g}')^T J\, \mathbf{g}' = J.$$

The basic step of the algorithm consists of the composition of two elementary symplectic maps. We present these maps in the case $d = 1$, that is, for $H(q,p) = A(p) + U(q) : \mathbb{R}^2 \to \mathbb{R}$, in which case our system is

$$\begin{aligned} \dot{q} &= \tfrac{\partial H}{\partial p} = A'(p) \\ \dot{p} &= -\tfrac{\partial H}{\partial q} = -U'(q). \end{aligned} \tag{17}$$

The basic step easily generalizes to higher dimensional separable Hamiltonian systems.

Fix a step size τ. Let $\boldsymbol{\gamma}_\tau^U(q,p) = (q, p - \tau U'(q))$. Note that $\boldsymbol{\gamma}_\tau^U$ is symplectic as its Jacobian satisfies

$$\begin{bmatrix} 1 & -\tau U''(q) \\ 0 & 1 \end{bmatrix} \begin{bmatrix} 0 & 1 \\ -1 & 0 \end{bmatrix} \begin{bmatrix} 1 & 0 \\ -\tau U''(q) & 1 \end{bmatrix} = \begin{bmatrix} 1 & -\tau U''(q) \\ 0 & 1 \end{bmatrix} \begin{bmatrix} -\tau U''(q) & 1 \\ -1 & 0 \end{bmatrix} = \begin{bmatrix} 0 & 1 \\ -1 & 0 \end{bmatrix}.$$

Similarly, the map $\boldsymbol{\gamma}_\tau^A(q,p) = (q + \tau A'(p), p)$ is symplectic. The composition $\boldsymbol{\gamma}_\tau^A \circ \boldsymbol{\gamma}_\tau^U$

$$\begin{bmatrix} q_n \\ p_n \end{bmatrix} \overset{\gamma_\tau^U}{\rightsquigarrow} \begin{bmatrix} \overline{q}_n \\ \overline{p}_n \end{bmatrix} = \begin{bmatrix} q_n \\ p_n - \tau \left.\frac{dU}{dq}\right|_{q_n} \end{bmatrix} \overset{\gamma_\tau^A}{\rightsquigarrow} \begin{bmatrix} q_n + \tau \left.\frac{dA}{dp}\right|_{\overline{p}_n} \\ p_n - \tau \left.\frac{dU}{dq}\right|_{q_n} \end{bmatrix} = \begin{bmatrix} q_{n+1} \\ p_{n+1} \end{bmatrix}$$

is a symplectic map which serves as the basic step (that is, one step) of the algorithm. This integration method is known as a "drift-kick" method.

For the harmonic oscillator with $k = m = 1$, $A(p) = \frac{1}{2}p^2$ and $U(q) = \frac{1}{2}q^2$. The basic step yields

$$\begin{bmatrix} q_n \\ p_n \end{bmatrix} \overset{\gamma_\tau^U}{\rightsquigarrow} \begin{bmatrix} q_n \\ p_n - \tau q_n \end{bmatrix} \overset{\gamma_\tau^A}{\rightsquigarrow} \begin{bmatrix} q_n + \tau(p_n - \tau q_n) \\ p_n - \tau q_n \end{bmatrix} = \begin{bmatrix} 1 - \tau^2 & \tau \\ -\tau & 1 \end{bmatrix} \begin{bmatrix} q_n \\ p_n \end{bmatrix}, \tag{18}$$

precisely the map given in (15). We see this symplectic basic step provides for an order 1 (in τ) algorithm.

More generally, an integration method is *order* r if the difference between the actual solution values and the approximating values at time t_n are $\mathcal{O}(\tau^r)$ as $\tau \to 0$, for t_n ranging in a bounded interval [21, §3.1].

Symplectic integration algorithms exist for any given even order in τ [25]. The algorithm used for our simulations has order 4, which can be arrived at by manipulating the above basic step as follows.

Definition. A one-step integration algorithm $\boldsymbol{\Psi}_\tau$ is *symmetric* if $\boldsymbol{\Psi}_\tau \circ \boldsymbol{\Psi}_{-\tau} = \mathbf{id}$, where **id** denotes the identity map.

It is easy to check that neither Euler's method (14) nor the symplectic basic step (18), when applied to the harmonic oscillator, is a symmetric method.

One useful property of symmetric integration algorithms is that they must be of even order in the step size [11, §2.3]. We turn the symplectic basic step (18) into a symmetric method by setting

$$\mathbf{\Gamma}_\tau = \boldsymbol{\gamma}^U_{\tau/2} \circ \boldsymbol{\gamma}^A_\tau \circ \boldsymbol{\gamma}^U_{\tau/2}. \tag{19}$$

This algorithm is clearly symmetric as

$$\mathbf{\Gamma}_\tau \circ \mathbf{\Gamma}_{-\tau} = (\boldsymbol{\gamma}^U_{\tau/2} \circ \boldsymbol{\gamma}^A_\tau \circ \boldsymbol{\gamma}^U_{\tau/2}) \circ (\boldsymbol{\gamma}^U_{-\tau/2} \circ \boldsymbol{\gamma}^A_{-\tau} \circ \boldsymbol{\gamma}^U_{-\tau/2}) = \mathbf{id}.$$

The simple trick (19) converts the symplectic basic step (18) into an order-2 SIA, albeit one now consisting of three compositions.

Though details fall beyond the scope of this article, Yoshida proved that any symmetric, order-$2n$ symplectic integrator $\mathbf{\Psi}_{2n}(\tau)$ can be used to create a symmetric, order $2n+2$ symplectic integrator $\mathbf{\Psi}_{2n+2}(\tau)$ [24]. This is accomplished by setting

$$\mathbf{\Psi}_{2n+2}(\tau) = \mathbf{\Psi}_{2n}(\alpha_1\tau) \circ \mathbf{\Psi}_{2n}(\alpha_0\tau) \circ \Psi_{2n}(\alpha_1\tau), \text{ where}$$

$$\alpha_0 = \frac{-2^{1/(2n+1)}}{2 - 2^{1/(2n+1)}} \quad \text{and} \quad \alpha_1 = \frac{1}{2 - 2^{1/(2n+1)}}.$$

Thus, to convert the algorithm given by basic step (19) into an order-4 method, we set $\mathbf{\Psi}_\tau = \mathbf{\Gamma}_{\alpha_1\tau} \circ \mathbf{\Gamma}_{\alpha_0\tau} \circ \mathbf{\Gamma}_{\alpha_1\tau}$, with $\alpha_0 = -2^{1/3}/(2 - 2^{1/3})$ and $\alpha_1 = 1/(2 - 2^{1/3})$. Though each step in the algorithm now entails composing nine symplectic maps, it is still relatively easy to program. This is the algorithm executed in *Matlab* and used by the first author to generate our Poincaré map orbits for the trilinear 3-body problem.

7. Fractals in the 3-Body Problem. The KAM Theory, named after A. Kolmogorov, V.I. Arnold, and J. Moser, and concerning the dynamics of area preserving perturbations of area preserving maps, provides another framework for the study of the trilinear 3-body problem. This is the approach taken in [15], to which we refer the reader for technical details supporting the observations below.

To a large extent the KAM Theory provides the mathematical underpinnings needed to substantiate Poincarés fundamental insight that chaotic behavior and fractals can occur in the 3-body problem. We now present examples of this behavior and intricate geometry, via homoclinic points and elliptic island chains, in the figures below.

Recall the Poincaré map P_a for the trilinear 3-body problem introduced in section 3. We select an initial condition of the form $(a, 0)$ for the large mass, and plot the

position and velocity (q_3, p_3) of the negligible mass each time the velocity of the large mass equals zero.

We note that the (q_1, q_3, p_1, p_3) restricted trilinear 3-body model, in which we set $m_3 = 0$ (equation (10)), is no longer Hamiltonian. Recall, however, that the (q_1, p_1) subsystem in equation (10) is Hamiltonian. We thus integrate for q_1 and p_1 precisely as described in section 6. In this fashion we consider the periodic function $q_1(t)$ to be a known entity. The values for q_1 can then be used to symplectically integrate for q_3 and p_3 in system (10). That is, the algorithm first updates the (q_1, p_1)-values, and then integrates for the (q_3, p_3)-values.

Figures 9, 10 and 11 provide striking visual evidence highlighting the superiority of the SIA to the Runge-Kutta algorithm. Both methods used are order 4, and each uses the exact same set of initial conditions, step size, and total integration time. As expected, the SIA provides for a much more detailed rendering of the long-time, global, qualitative structure in the (q_3, p_3)-plane.

What of chaotic behavior? Notice the dense concentration of points roughly near $(1.3, 0)$ and $(-1.3, 0)$ in Figure 9. This is evidence of chaotic behavior due to the existence of homoclinic points. Poincaré himself coined the term *homoclinic* for points whose orbits were both forward and backward asymptotic to the same periodic point. He clearly realized that the existence of such points could lead to complicated orbit behavior via "stretching and folding," considered in modern times as the hallmark of systems with chaotic behavior. It was through the work of G. Birkhoff in the early 20th century and S. Smale in the 1960s that chaotic behavior was proven to exist in the presence of homoclinic points, work which involved fractal Cantor sets, symbolic dynamics, and Smale's horseshoe map. These chaotic orbits are prevalent in Figure 10.

The KAM Theory can also be used to explain the existence of the fractal structure inherent in nested sequences of *elliptic island chains* [15]. An elliptic periodic point for the map P_a is a periodic point which is surrounded by invariant (under an iterate of P_a), simple closed curves in the (q_3, p_3)-plane. Several elliptic periodic points are evident in Figures 9-16 via their surrounding invariant curves. (The periodic points are in the centers of these families of curves.)

An elliptic island chain consists of alternating elliptic and saddle periodic points within an annular region. For small area preserving perturbations of area preserving maps, there are infinitely many elliptic periodic points, each surrounded by such island chains, on ever smaller scales ([13], [2, §6.5]).

In Figure 12 we see the coexistence of chaotic orbits and a rich, global, qualitative structure. Zooming in near the point $(0.45, 0)$ yields Figure 13, where the chains of

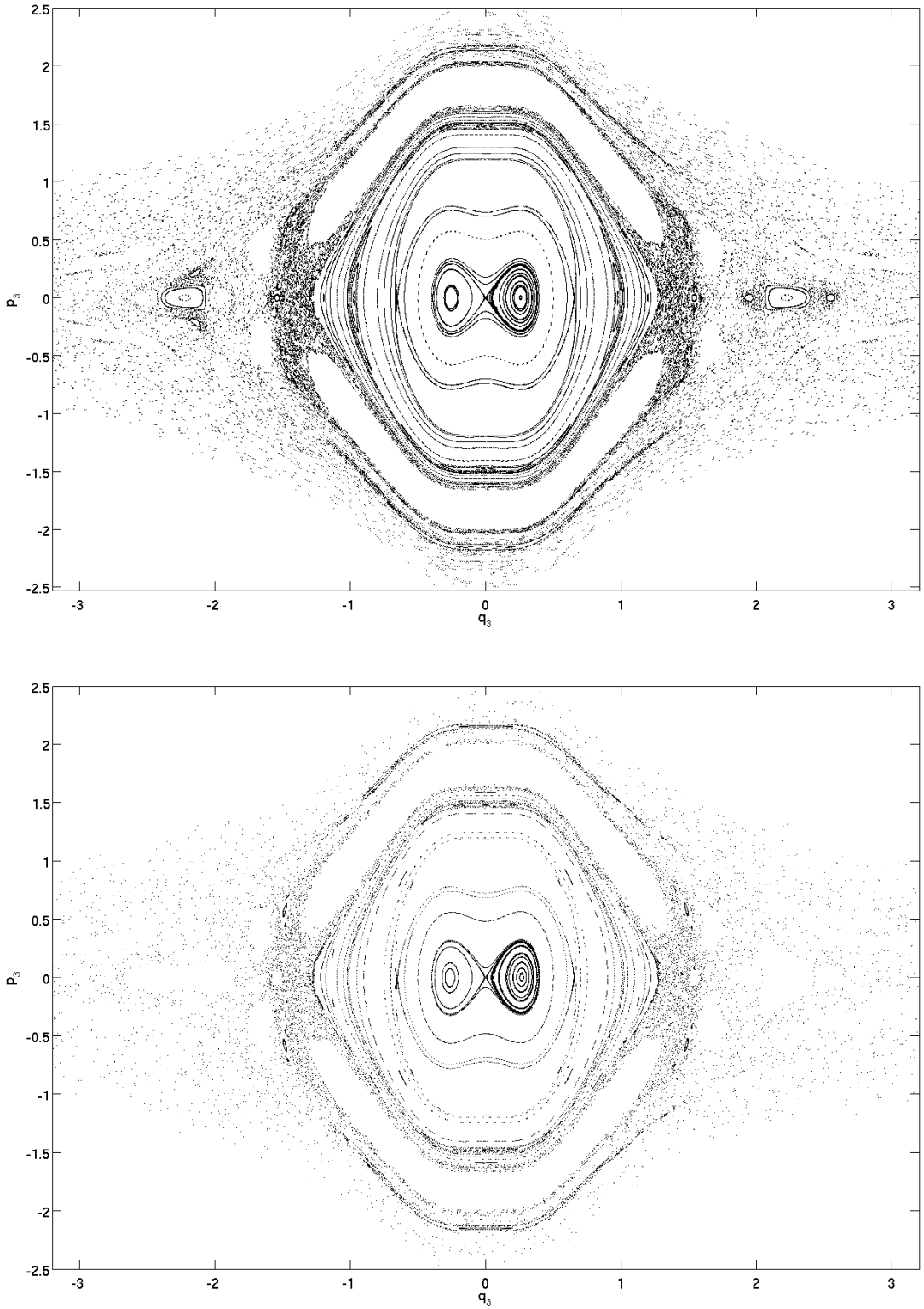

Figure 9. Fixed time step ($\Delta t = 0.006$), with the same 83 initial conditions, computing the position and velocity of the small mass out to $t = 2800$ each time the large mass has velocity zero. The parameter $a = 1/(2\sqrt{2})$. Top: fourth order symplectic integration algorithm. Bottom: fourth order Runge-Kutta algorithm.

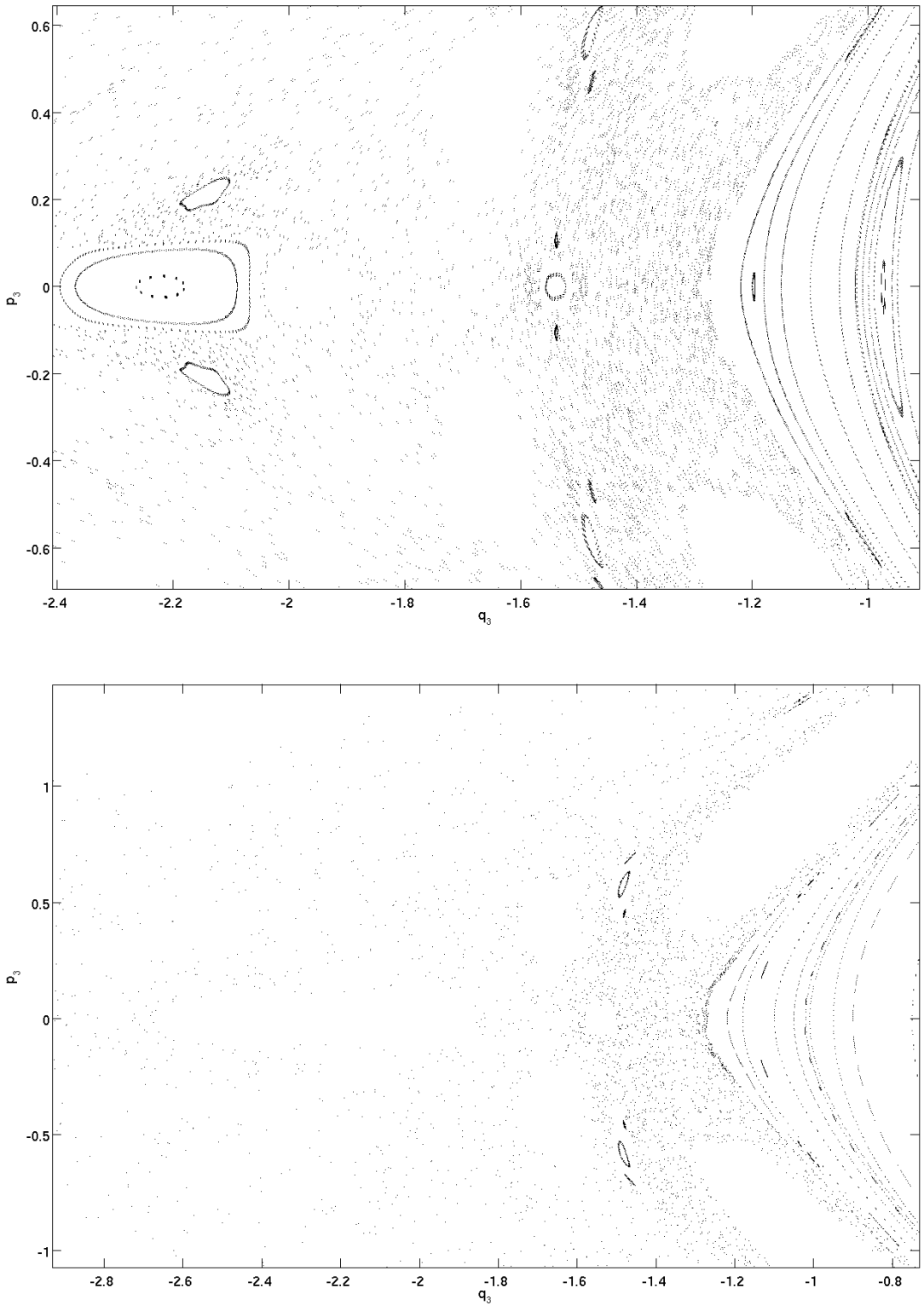

Figure 10. As in Figure 9. Top: fourth order symplectic integration algorithm. Bottom: fourth order Runge-Kutta algorithm.

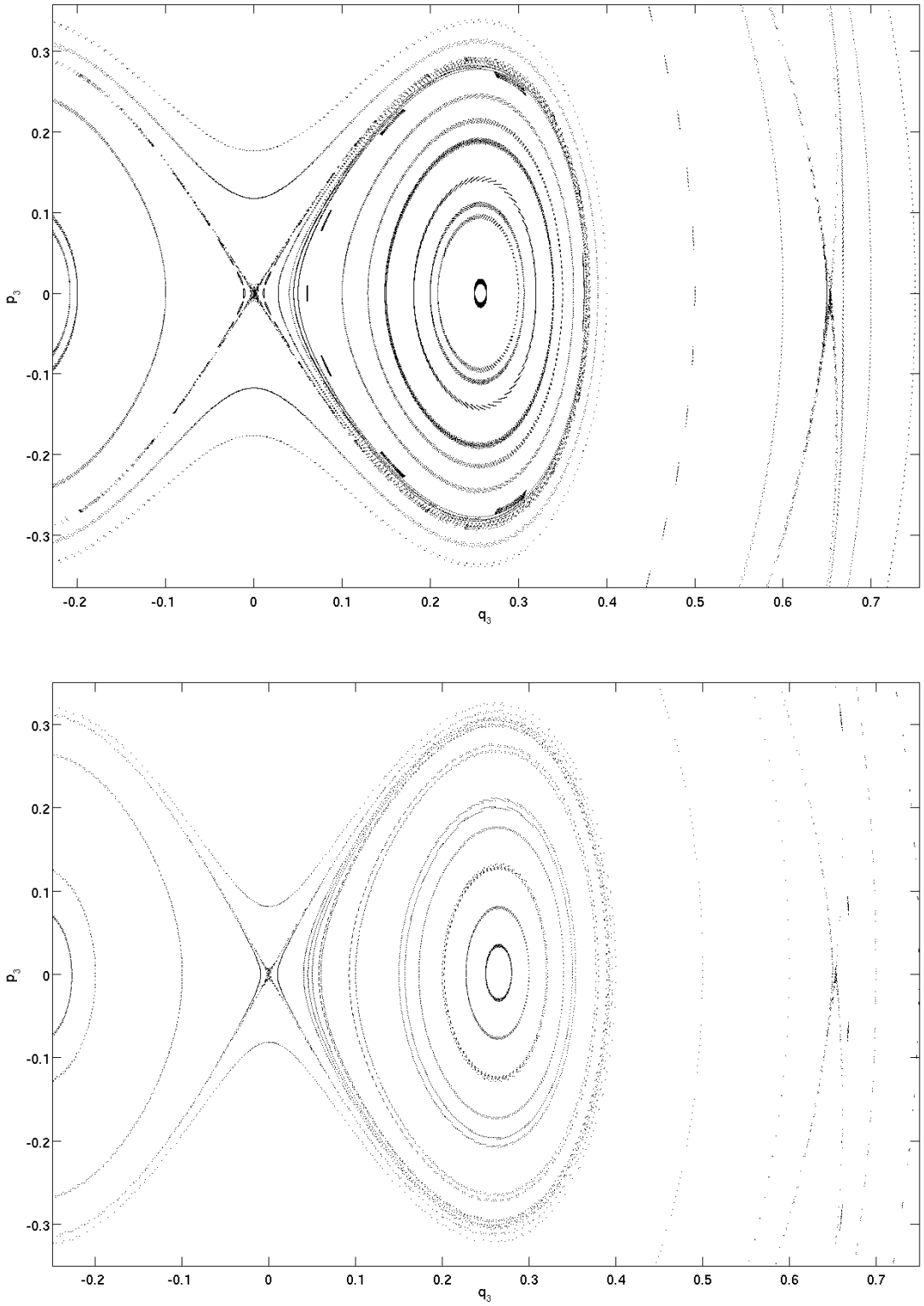

Figure 11. As in Figure 9. Top: fourth order symplectic integration algorithm. Bottom: fourth order Runge-Kutta algorithm.

elliptic islands are clearly evident. A closer inspection of a neighborhood of the origin in Figure 12 yields Figure 14. The elliptic island chains would continue to appear as one continued to zoom in on various portions of the (q_3, p_3)-plane, providing further evidence of the efficacy of the symplectic integration algorithm in uncovering this fractal structure.

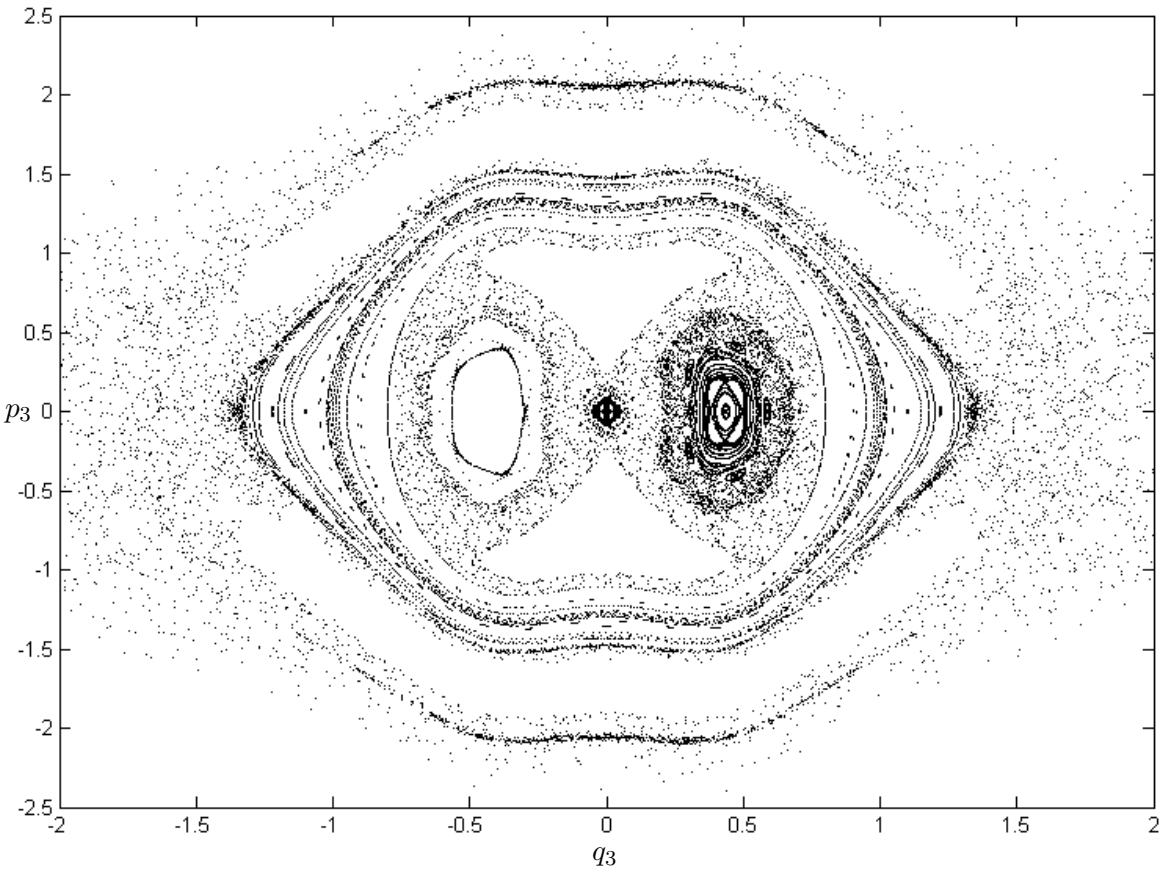

Figure 12. Orbits of the Poincaré map P_a, $a = 0.4325$ (300,000 iterates for each of roughly 100 initial conditions).

The generation of ergodic orbits, that is, those densely filling regions in the (q_3, p_3)-plane, is also remarkably well done by the SIA. Notice how these orbits clearly avoid the embedded stable regions and elliptic island chains in Figures 15 and 16.

8. Conclusion. From an historical perspective, the n-body problem is the central problem in the field of dynamical systems. Via the trilinear 3-body problem, we have been able to introduce undergraduates to some of the beautiful mathematics and remarkable images generated through its study. We have provided a relatively

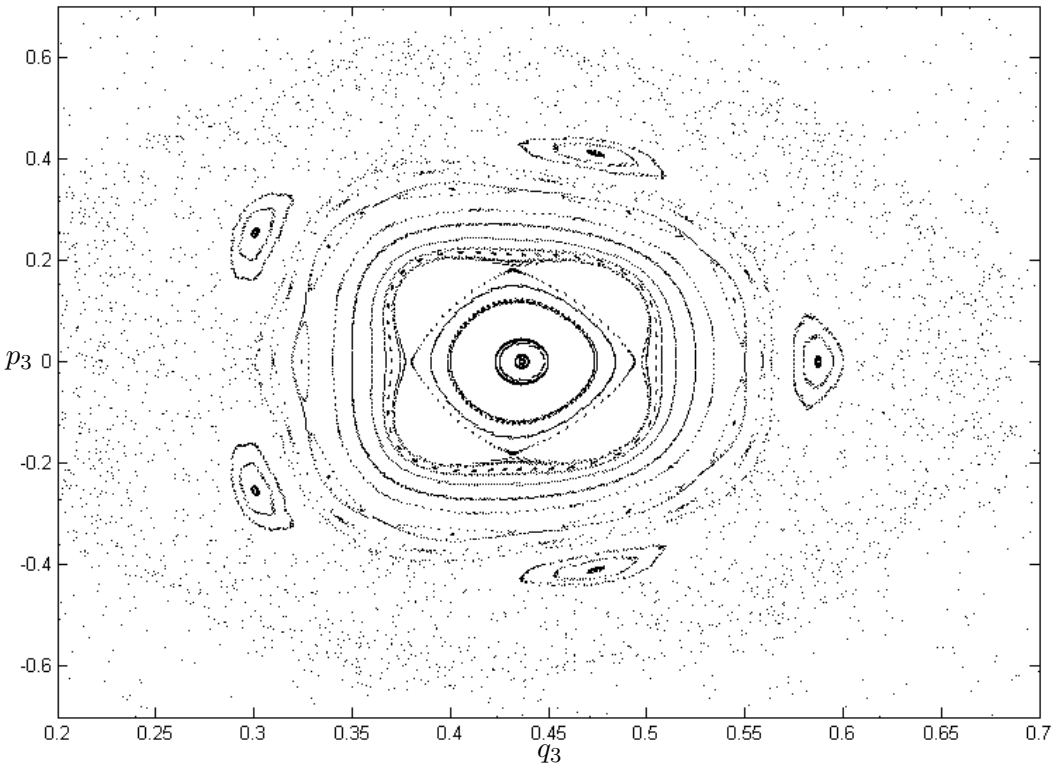

Figure 13. Zooming in on the region near $(0.45, 0)$ in Figure 12. Note the many elliptic island chains.

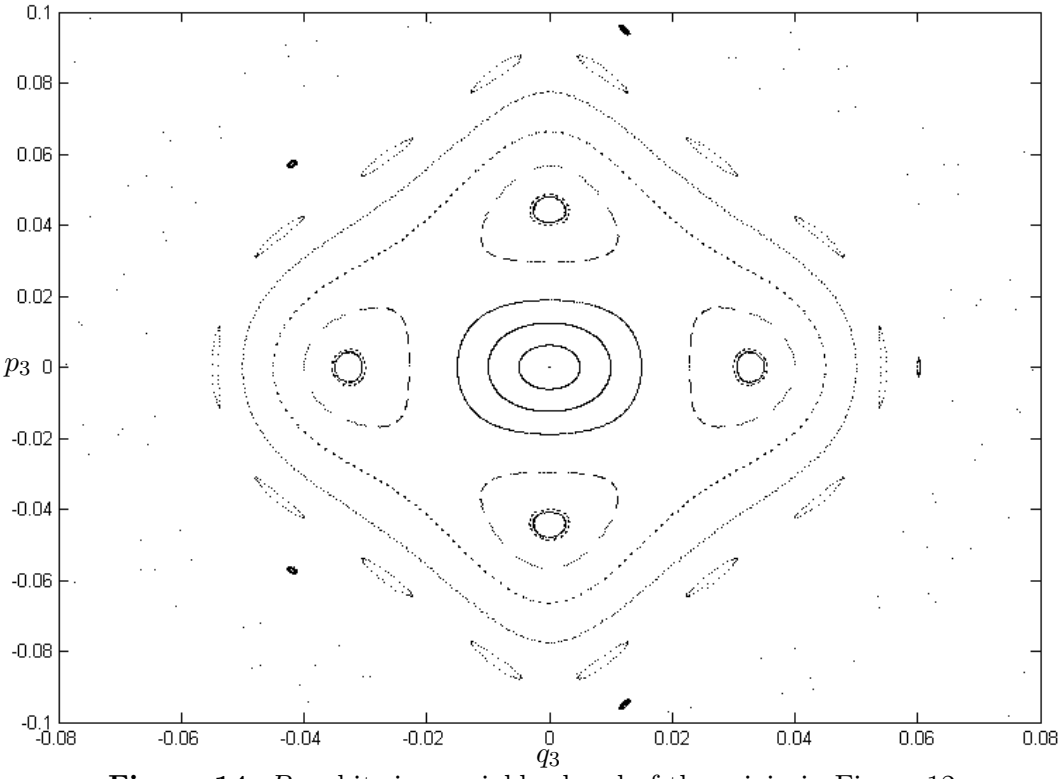

Figure 14. P_a-orbits in a neighborhood of the origin in Figure 12.

elementary introduction to the notion of symplectic maps, their relationship to Hamiltonian systems of ODEs, and their use as the basis for a symplectic integration algorithm. We have used the SIA to unearth fractal structure and chaotic dynamics in the trilinear 3-body problem, as Poincaré would have done had he access to our modern tools.

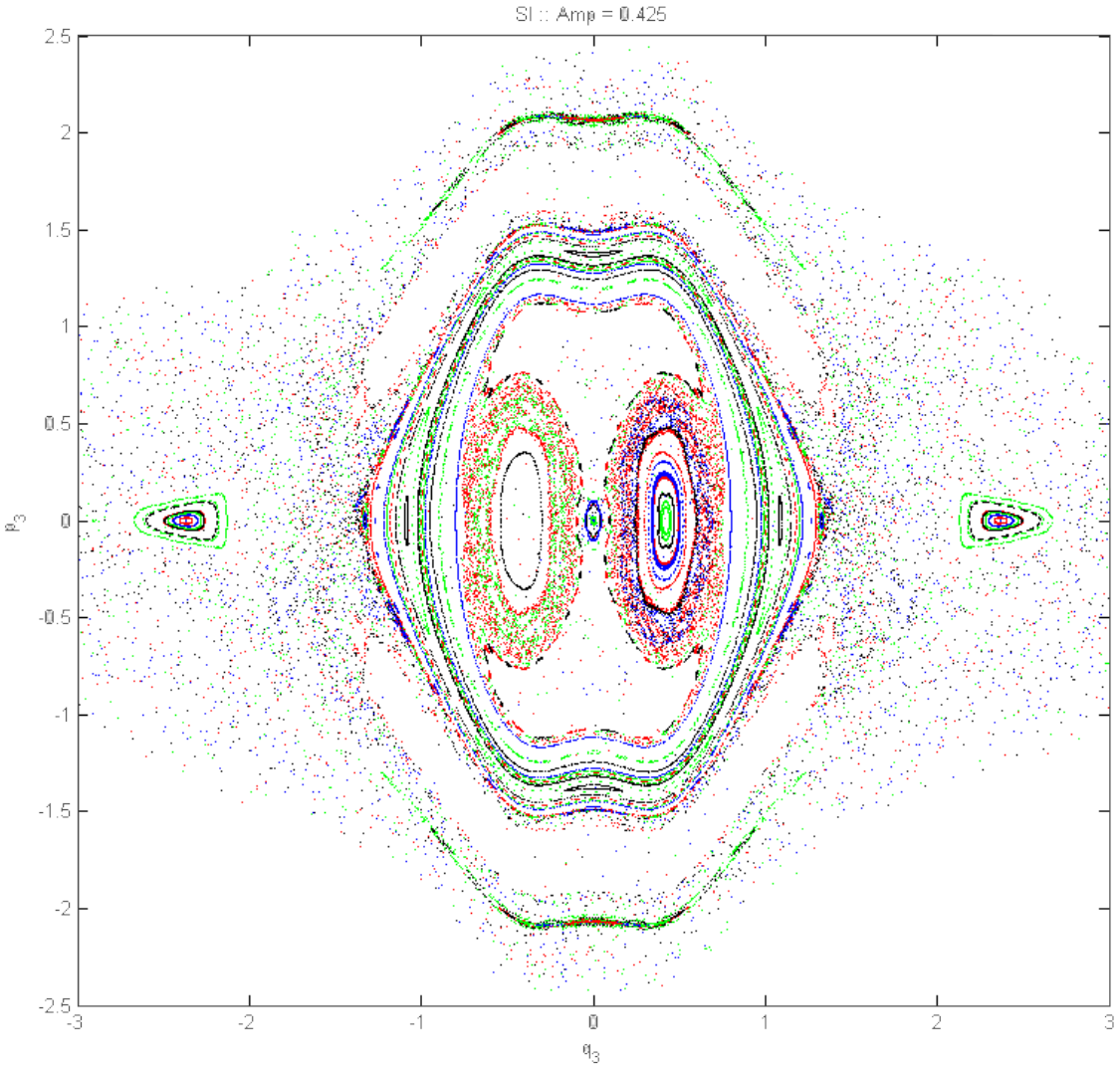

Figure 15. The ergodic orbits of P_a avoid the stable regions ($a = 0.425$).

The SIA is clearly superior to the Runge-Kutta algorithm when integrating Hamiltonian systems of ODEs as it is designed to conserve energy (see Figure 17). This implies the SIA is ideally suited to generate long-time integrations, which are necessary if one is interested in the global qualitative structure of phase space. New insights into the dynamics of the n-body problem and fractal structure in the phase

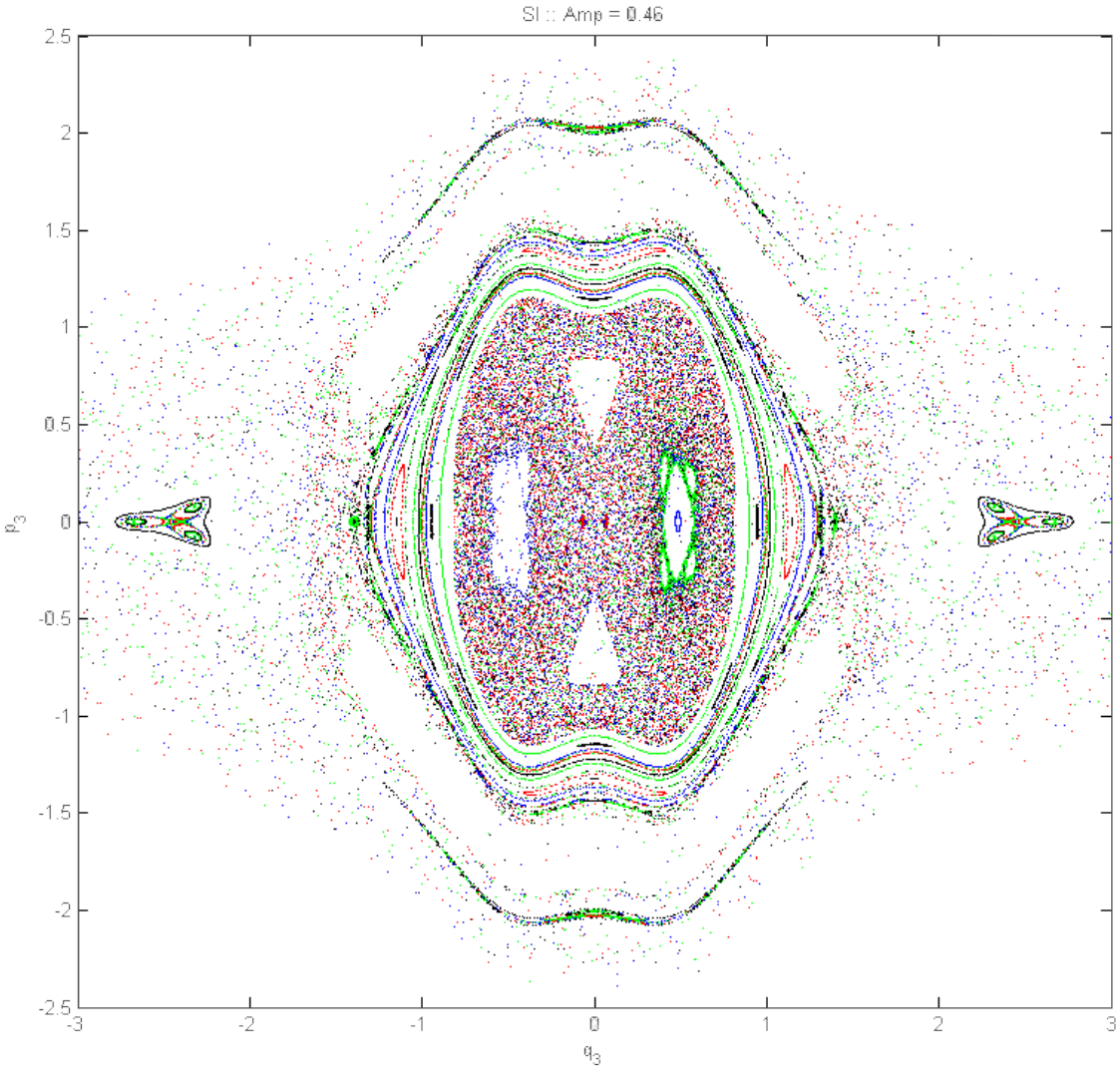

Figure 16. The ergodic orbits of P_a are well-rendered by the SIA ($a = 0.46$).

space will continue to be revealed through the ongoing development and use of symplectic integration algorithms.

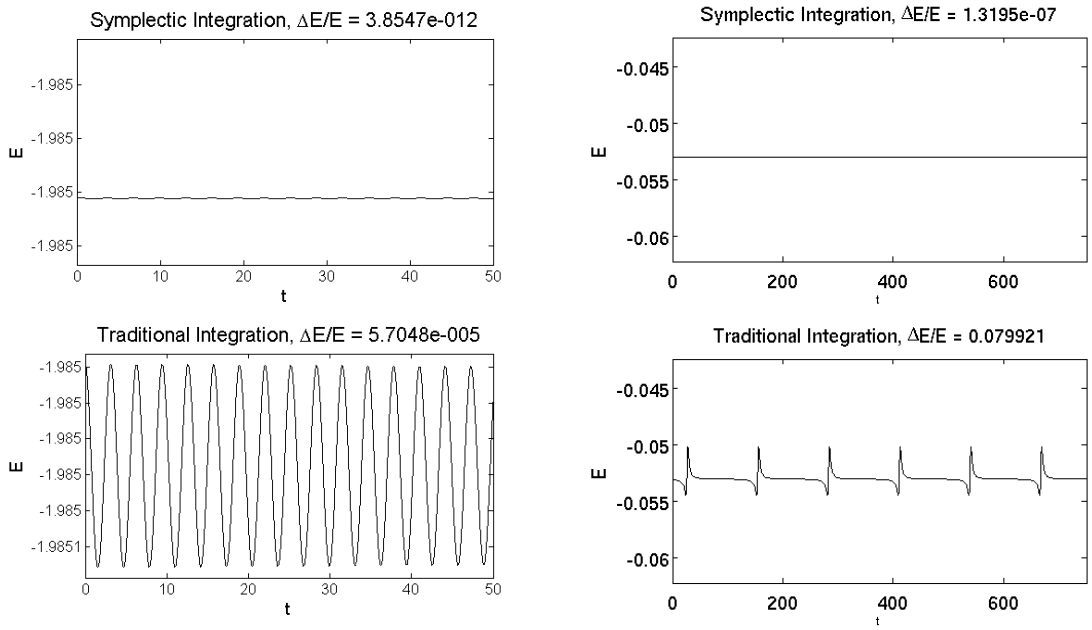

(a) (b)

Figure 17. Comparison of energy conservation between symplectic integration (top) and Runge-Kutta (bottom). (a) For the ideal pendulum. (b) For the two-dimensional 2-body problem.

References.

1. Arnold, V.I., *Mathematical Methods of Classical Mechanics*, New York, NY: Springer-Verlag (1989).

2. Arrowsmith, D.K., Place, C.M., *An Introduction to Dynamical Systems*, Cambridge, UK: Cambridge University Press (1990).

3. Blanchard, P., Devaney, R.L., Hall, G.R., *Differential Equations*, Pacific Grove, CA: Brooks/Cole (2006).

4. Borrelli, R., Coleman, C., *Differential Equations A Modeling Perspective*, New York, NY: Wiley (2004).

5. Channell, P.J., Scovel, C., Symplectic integration of Hamiltonian systems, *Nonlinearity* **3** (1990), 231-259.

6. Chin, S.A., A fundamental theorem on the structure of symplectic integrators,

Physics Letters A 354 (2006), 373-376.

7. Chin, S.A., Chen, C., Fourth order gradient symplectic integrator methods for solving the time-dependent Schrödinger equation, *J. of Chemical Physics* **114** (17) (2001), 7338-7341.

8. Chin, S.A., Kidwell, D., Higher-order force gradient symplectic algorithms, *Physical Review E* **62** (6) (2000), 8746-8752.

9. Creutz, M., Gocksch, A., Higher-order hybrid Monte Carlo algorithms, *Physical Review Letters* **63** (1) (1989), 9-12.

10. Forest, E., Ruth, R., Fourth-order symplectic integration, *Physica D* 43 (1990), 105-117.

11. Hairer, E., Lubich, C., Wanner, G., *Geometric Numerical Integration*, New York, NY: Springer (2006).

12. Hartman, P., *Ordinary Differential Equations*, Boston, MA: Birkhäuser (1982).

13. Hénon, M., Numerical exploration of Hamiltonian systems, in *Comportement Chaotique des Systèmes Déterministes: Les Houches, Session XXXVI, 1981*, eds. Iooss, G., Helleman, R.H.G & Stora, R., New York, NY: North Holland (1983).

14. Hirsch, M., Smale, S., Devaney, R.L., *Differential Equations, Dynamical Systems, & an Introduction to Chaos*, San Diego, CA: Academic Press (2004).

15. Lodge, G., Walsh, J.A., Kramer, M., A trilinear three-body problem, *International Journal of Bifurcation & Chaos* **13** (8) (2003), 2141-2155.

16. Meyer, K., Hall, G.R., *Introduction to Hamiltonian Dynamical Systems and the N-body Problem*, New York, NY: Springer-Verlag (1992).

17. Moore, C., Nauenberg, M., New periodic orbits for the n-body problem, *Journal of Computational and Nonlinear Dynamics* **1** (4) (2006), 307-311.

18. Murray, N., Holman, M., The origin of chaos in the solar system, *Science* **283** (1999), 1877-1881.

19. Poincaré, H., Sur le problème des trois corps et les équations de la dynamique, *Acta* 13 (1890), 1-270.

20. Poincaré, H., *Les Méthodes Nouvelles de la Mécanique Céleste. Tome III*, Paris: Gauthiers-Villars (1899).

21. Sanz-Serna, J.M., Calvo, M.P., *Numerical Hamiltonian Problems*, London, UK: Chapman & Hall (1994).

22. Scuro, S., Chin, S.A., Forward symplectic integrators and the long-time phase error in periodic motions, *Physical Review E* **71** (2005), 056703-1 – 056703-12.

23. Sussman, G., Wisdom, J., Chaotic evolution of the solar system, *Science* **257** (1992), 56-62.

24. Yoshida, H., Construction of higher order symplectic integrators, *Physics Letters A* **150** (1990), 262-268.

25. Yoshida, H., Symplectic integrators for Hamiltonian systems: basic theory, in *Chaos, Resonance, and Collective Dynamical Phenomena in the Solar System: Proceedings of the 152nd Symposium of the International Astronomical Union*, S. Ferraz-Mello ed., Boston, MA: Kluwer (1992).